Binary Pseudo-Random Array for Calibration of Interferometers with Transmission Spheres and Cylinders

K. Munechika*[a], S. Rochester[b], W. Chao[c], I. Lacey[d], C. Pina-Hernandez[a], K. Yamada[a], M. P. Biskach[e], P. Takacs[f], U. Griesmann[g], and V. V. Yashchuk[d]

[a]HighRI Optics, Inc., 5401 Broadway Terr, St. 304, Oakland, California 94618, USA; [b]Rochester Scientific, LLC, 2041 Tapscott Avenue, El Cerrito, CA 94530, USA; [c]Center for X-ray Optics, Lawrence Berkeley National Laboratory, Berkeley, CA 94720, USA; [d]Advanced Light Source, Lawrence Berkeley National Laboratory, Berkeley, CA 94720, USA; [e]NASA Goddard Space Flight Center, 8800 Greenbelt Road, Greenbelt, MD 20771 USA; [f]Surface Metrology Solutions LLC, 19 S 1st St, Unit B901, Minneapolis, MN 55401 USA; [g]National Institute of Standards and Technology, Sensor Science Division, Gaithersburg, MD 20899, USA

ABSTRACT

Binary pseudo-random array (BPRA) "white noise" artifacts are highly effective for characterizing the instrument transfer function (ITF) of surface topography metrology tools and wavefront measurement instruments. These BPRA artifacts feature all spatial frequencies within the instrument bandpass equally, resulting in a power spectral density with a white-noise-like character. This characteristic allows for direct ITF determination with uniform sensitivity across the entire spatial frequency range. We have developed a novel BPRA calibration standard that combines the diffractive pattern of a reflection computer-generated hologram (CGH) with the white noise generating BPRA pattern. By integrating these technologies using the same lithographic techniques, the resulting calibration sample enables ITF characterization of a Fizeau interferometer with a transmission sphere, or any nulling optic.

Keywords: calibration, instrument transfer function, ITF, power spectral density, PSD, interferometric microscopes, binary pseudo-random, test standard, aberration, surface metrology

1. INTRODUCTION

High-accuracy metrology is vitally important in the manufacture and use of ultra-high-quality free-form mirrors designed, for example, for space x-ray telescopes to manipulate x-ray light with nanometer-scale wavelengths. Due to the shorter wavelength, requirements on the surface figure (shape) and finish (roughness) of x-ray mirrors are many orders of magnitude more stringent than for visible-light optics. Additionally, because practically all optical materials are transparent to x-ray light at normal incidence, grazing incidence is used to achieve acceptable reflectance. This results in additional complications for metrology. To achieve an acceptable optical aperture, the x-ray mirrors are elongated in the tangential direction and are often strongly aspherical with a tangential best-fit radius of curvature (ROC) that can exceed the sagittal ROC by orders of magnitude. Correspondingly, the metrology integrated into x-ray mirror manufacturing must ensure the accuracy of optical surface fabrication at the sub-nanometer level over large, meter-long aspherical optical elements with sagittal ROCs on the order of a meter and less, whereas the tangential ROCs can reach several hundred meters.

Metrology technology has not kept up with the advancement in fabrication technologies. It is the deficiencies in the metrology, rather than the fabrication technologies that primarily limit the optical quality. For example, the micro-stitching metrology used in the elastic emission machining (EEM) deterministic nano-fabrication process [1-3] produces aberration errors that depend on the surface curvature. Such errors are often transferred into the optical surface topography of x-ray mirrors, where they result in quasi-periodic errors in the surface height and slope [4]. Therefore, advanced integrated metrology is key for the improvement of optical manufacturing technology, urgently needed for fabrication of free-form aspherical x-ray mirrors with moderately and strongly curved shapes, such as paraboloids, ellipsoids, hyperbolas,

* Corresponding author: km@highrioptics.com; phone 1-(800) 470-7902; https://highrioptics.com/

diaboloids, and others. We present a novel method that combines computer-generated holograms (CGHs) and binary pseudo-random arrays (BPRAs) to facilitate the calibration of the instrument transfer function of a Fizeau interferometer with non-collimated test wavefront.

2. NOVEL APPROACH TO ENABLE INSTRUMENT TRANSFER FUNCTION CALIBRATION OF FIZEAU INTERFEROMETER EQUIPPED WITH TRANSMISSION SPHERE REFERENCE

Computer generated holograms (CGHs) are frequently used in interferometric tests as auxiliar optical elements to convert an interferometer wavefront into a custom-designed wavefront that matches the shape of a surface under test. Such stand-alone CGHs can be designed as transmission or as reflection elements, both fabricated on flat substrates [5].

We report the design and experimental realization of calibration standards that combines reflection CGHs to retro-reflect spherical or cylindrical wavefronts with a BPRA pattern. The calibration mirrors can be used to characterize the performance of Fizeau interferometers with transmission spheres for the testing of spherical surfaces, or cylindrical Fizeau objectives for cylindrical surfaces as shown in Fig. 1.

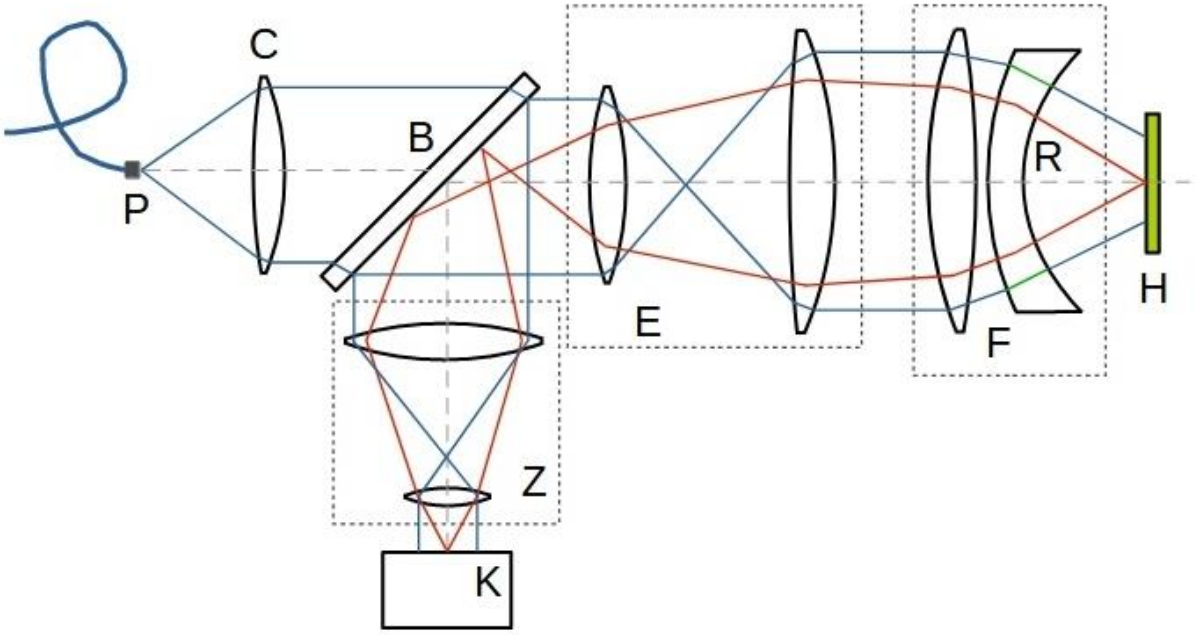

Figure 1: Schematic of a Fizeau interferometer with spherical or cylindrical Fizeau objective. Illumination rays are shown in blue, imaging rays in red. The components of the interferometer are light source (P), collimator (C), beam divider (B), beam expander (E), Fizeau objective, or transmission reference, (F) with reference surface (R), zoom objective (Z), and camera (K). In some applications the Fizeau objective may be replaced by a CGH, or a CGH may be used in addition to the Fizeau objective. A computer-generated reference hologram incorporating a BPRA pattern (H) is used to characterize the transfer function of the interferomet

We demonstrated the concept by developing a spherical CGH (SCGH) design to pair with an existing spherical transmission reference. The spherical reflection CGH design was developed by our collaborator at NIST and the CGH was fabricated on a Si wafer as described in Sec. 2.1. Parts of the combined CGH and BPRA patterns design are shown in Figure 2. Red areas are a part of the spherical CGH design, and blue squares are the elements of the highly-randomized (HR) BPRA design, with a element size of 35 x 35 μm^2.

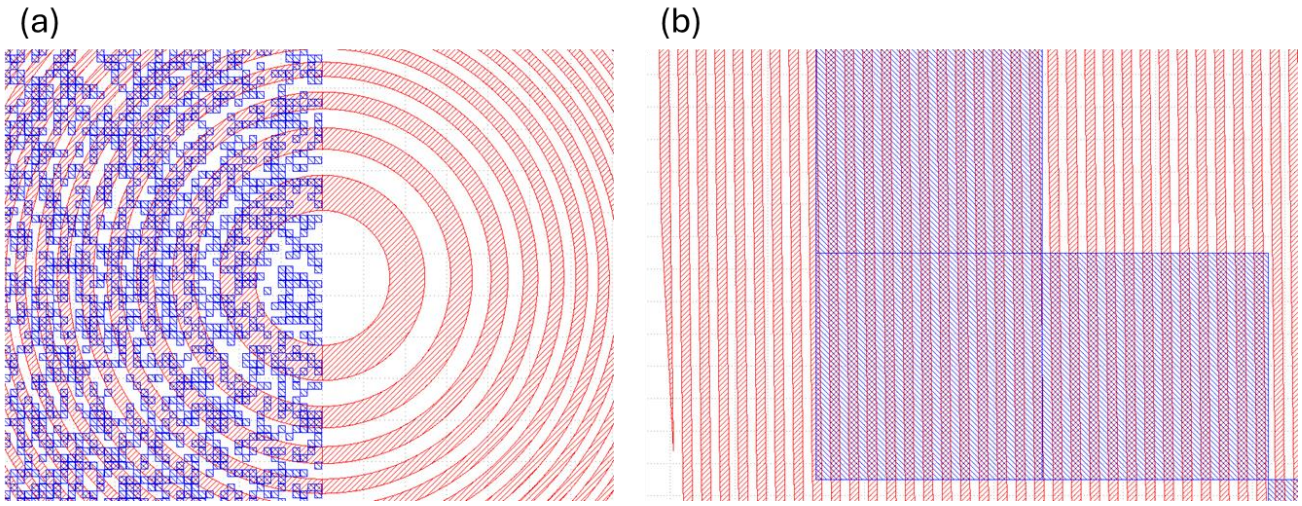

Figure 2 (a) Combined design for the spherical CGH (red) and HR BPRA (blue) (a) at the center of the CGH and (b) near the edge of the CGH. The smallest BPRA feature size (width of a single blue square) is 35 µm wide in (a) and (b). In (b), the period of the CGH pattern is much smaller than the BPRA feature size.

2.1 Fabrication of SCGH with the HR-BPRA pattern

The fabrication process for the SCGH sample patterned with the HR-BPRA is shown in Figure 3. The starting substrate is a standard silicon wafer. First, 80 nm of Cr was deposited on the wafer using electron beam evaporation. A positive photoresist was spin-coated to a thickness of 5 µm, and baked at 100° C for 5 minutes. Then, the photoresist was exposed to 365 nm UV light with a dose of 45 mJ/cm^2 through a photomask with the CGH pattern. Development in 0.26 molar tetra methyl ammonium hydroxide (TMAH) developer for 45 seconds created the CGH patterned photoresist. Another Cr evaporation with the thickness of 115 nm and lifting off the photoresist in n-methyl-2-pyrrolidone (NMP) created the reflective CGH on the substrate.

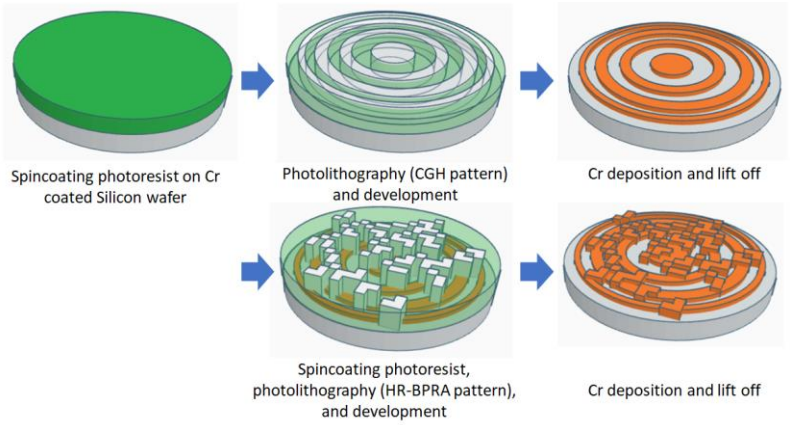

Figure 3 The CGH HR-BPRA fabrication process.

After initial evaluation of the reflective SCGH using a Fizeau interferometer with an f/2.2 transmission sphere at the Advanced Light Source (ALS) X-Ray Optics Laboratory (XROL), the HR-BPRA patterns were fabricated on top of the CGH pattern. The same photolithography process described before was performed using a HR-BPRA patterned photomask. After the development step, a HR-BPRA patterned photoresist layer was obtained on top of the reflective CGH sample. 80 nm of Cr was evaporated on it and lift off was performed to make the CGH HR-BPRA sample. Figure 4 shows a microscopic image and photograph of the fabricated CGH HR-BPRA sample. No alignment between the two layers was necessary. Two nominally identical mirrors were fabricated using the described process.

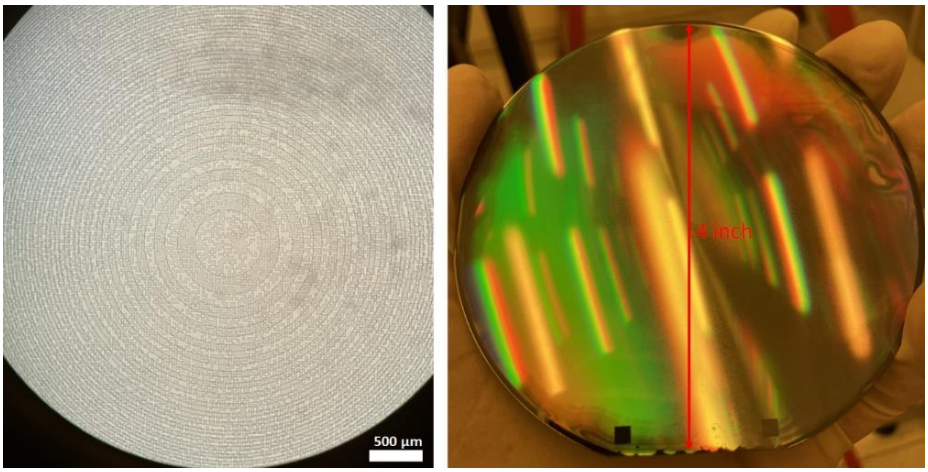

Figure 4 A microscope image (left) and photograph (right) of the fabricated CGH HR-BPRA sample.

3. CHARACTERIZATION OF THE CGH/BPRA SAMPLE WITH AN INTERFEROMETRIC MICROSCOPE

3.1 Microscope measurements after fabrication of the spherical CGH pattern

After fabrication of the two SCGH samples, the correspondence of the etched pattern to the CGH design was verified by a surface-height measurement with a coherence scanning interferometric (CSI) microscope. The results of the measurements are depicted in Figure 5. For the measurements, the microscope was equipped with a 20× objective. In this arrangement, the spatial resolution of the microscope is about 500 nm (see, for example, Ref. [1]), which is close to the effective detector pixel size of 434 nm. This resolution allows accurate measurement of the SCGH samples within a radius of about 25 mm from the pattern center. At larger distances from the pattern center, the SCGH pattern was characterized with a scanning electron microscope available at the LBNL Molecular Foundry. The optical microscope (Figure 4) and the SEM measurements are in good agreement, and both confirm that the spherical CGH pattern is of good quality, with a uniform depth of the desired value of about 125 nm.

3.2 Microscope measurements after fabrication of the HR-BPRA pattern on the wafers with spherical CGH

Additional surface-height measurements were made after fabrication of the HR-BPRA pattern atop the CGH pattern. Figure 6 and Figure 7 illustrate the results of the measurements. For the measurements in Figure 6, similar to the ones in Figure 5, the microscope was equipped with a 20× objective. In this arrangement, the depth of the BPRA pattern with the minimum feature size of 25 µm is measured to be ≈85 nm. Keeping in mind the double pass of the reflected light, this depth corresponds to $\approx\lambda/4$ optical path difference for the light reflected from the top and bottom surfaces of the BPRA pattern. The relatively large depth of the BPRA pattern is used in order to clearly discriminate the power spectral density (PSD) of the BPRA from that of the SCGH sample (see Sec. 2), because for the present proof-of-principle tests we used inexpensive Si wafers that have a large surface form error and are easily deformed.

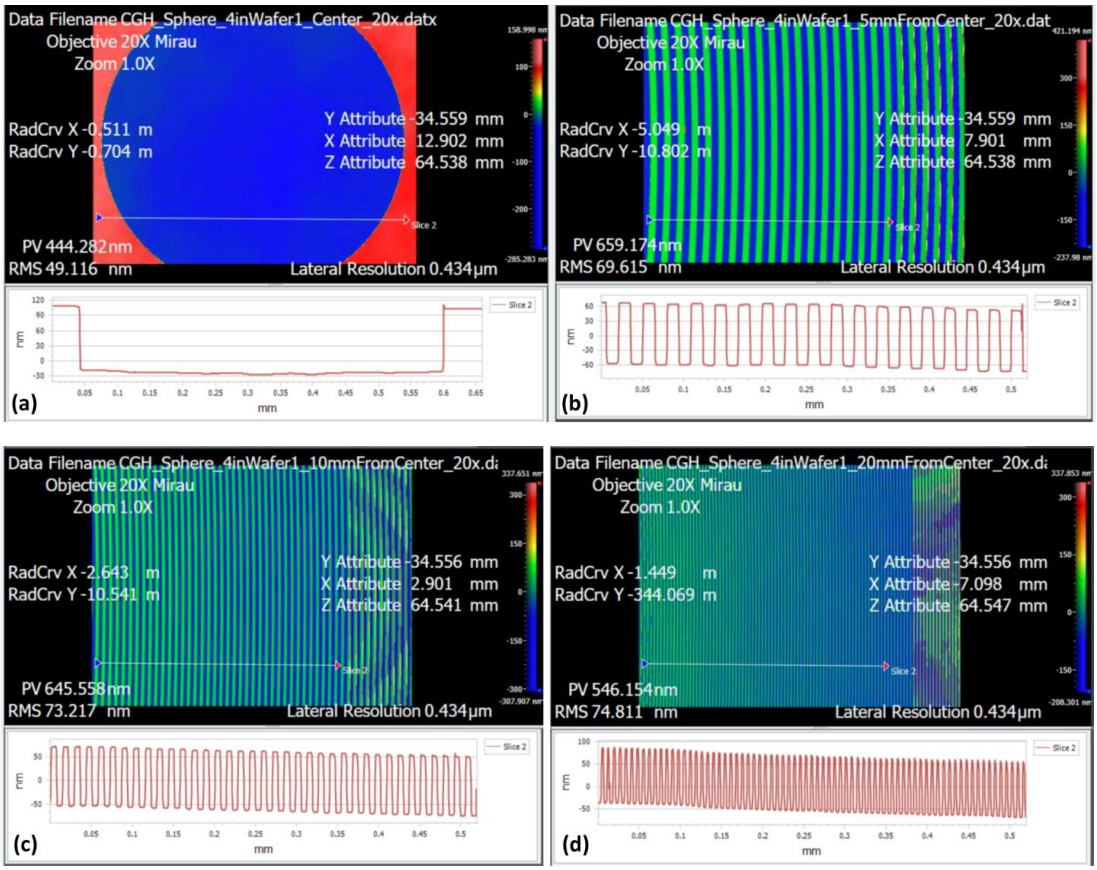

Figure 5: Surface height profile of the spherical CGH sample #1 as measured with the interferometric microscope at (a) the CGH pattern center, and at distances of (b) 5 mm, (c) 10 mm, and (d) 20 mm from the center. For the measurements, the microscope was equipped with a 20× objective for an effective detector pixel size of 434 nm. The best fit overall offsets (pistons) are removed.

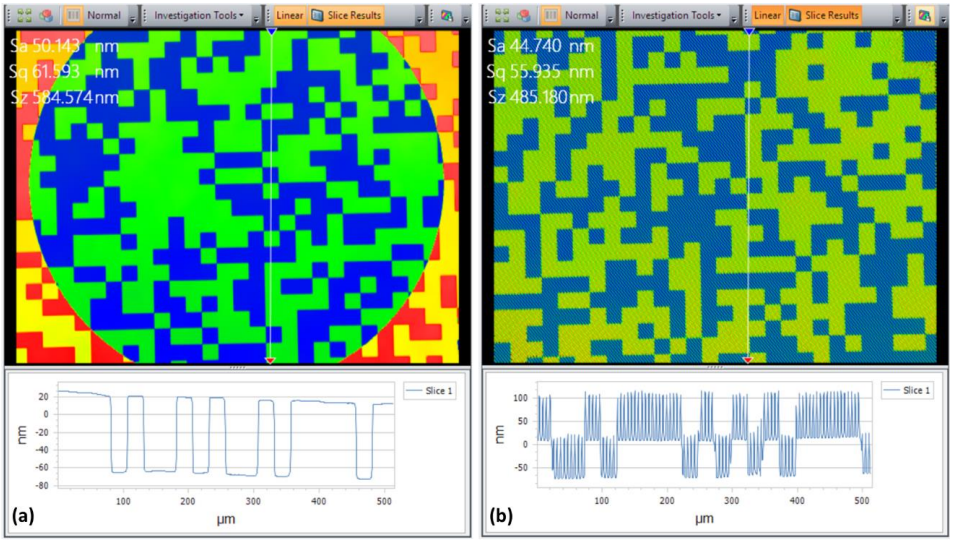

Figure 6: Surface height profile of the SCGH/BPRA sample #1 as measured with the CSI microscope (a) at the CGH pattern center (X = 0, Y = 0), and (b) at the position with the coordinates X ≈ 30 mm and Y ≈ 26 mm. The microscope arrangement was as for Figure 5. The surface measurements are detrended using the best fit planes.

Figure 7 depicts the surface height profile of the SCGH/BPRA sample #1 as measured with the CSI microscope equipped with a 2.75× objective resulting in an effective detector pixel size of 3.115 µm. The best fit plane is subtracted. The SCGH/BPRA overall concave spherical shape with radius of curvature of about 30 m is the result of the coating surface stress. Nevertheless, the stress related curvature is much smaller (by two orders of magnitude) than that of the desired wavefront curvature of the SCGH and does not affect the results of the tests with a Fizeau interferometer discussed in Sec. 4, below. The results of the interferometric microscope measurements with the SCGH/BPRA sample #2 are essentially the same as those presented in this section for sample #1.

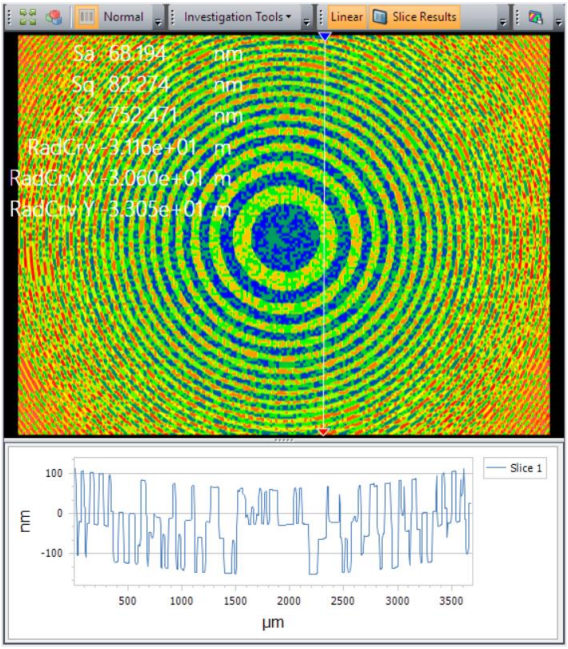

Figure 7 The surface height variations of the SCGH/BPRA sample #1 as measured with the coherence scanning interference microscope at the pattern center. The microscope was equipped with a 2.75× objective resulting in a detector pixel size of 3.115 µm. The best fit plane is subtracted.

4. CHARACTERIZATION OF THE SPHERICAL CHG/BPRA SAMPLE WITH A FIZEAU INTERFEROMETER

4.1 Experimental arrangement

Figure 8 shows the experimental arrangement of the Fizeau interferometer measurements with the spherical CGH samples before and after fabrication of the HR-BPRA patterns. For the measurements we used a Fizeau interferometer equipped with a f/2.2 spherical transmission reference with focal length of 335.6 mm.

4.2 Zero-order measurements with the spherical CGH samples before fabrication of the HR-BPRA pattern using plane-wavefront Fizeau interferometry

For a preliminary characterization of the SCGH sample surface quality, we measured the samples in zeroth-order with the Fizeau interferometer equipped with a transmission flat. Figure 9 presents the shape of the SCGH sample #2 as measured in the zeroth-order setup. The best fit plane surface is removed.

The measurement confirms the overall concave spherical shape of the SGCH samples caused by the surface stress due to the coating. A similar shape was observed in the interferometric microscope measurements over a small central area of sample #1. The zeroth-order surface images, like the one in Figure 9, help us to better understand the quality of the SCGH samples. In a perfectly made phase SCGH, the zeroth order would not exist. Therefore, with the SCGH developed on a low-cost wafer, the plano zeroth-order reflection is expected to be very small, with the spherical fringe system

predominantly diffracting into the first order. Thus, the very low contrast of the nearly plano fringe pattern in Figure 9 can be thought of as a confirmation of the good fabrication quality of the SCGH samples.

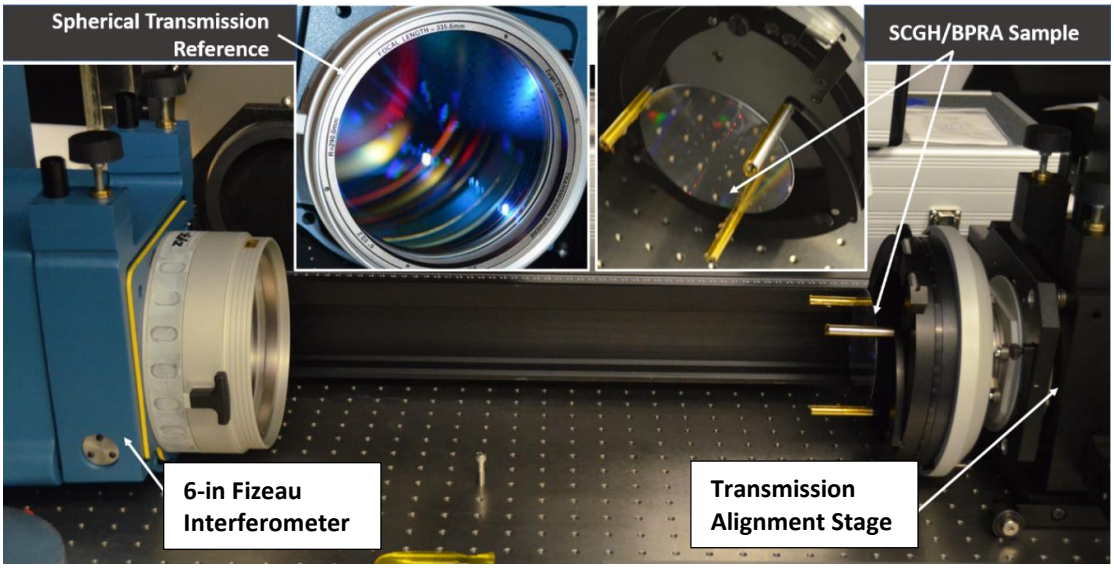

Figure 8: Experimental setup of the Fizeau interferometer equipped with a spherical transmission reference, used for the first diffraction order measurements with the spherical CGH samples before and after patterning with the HR-BPRA.

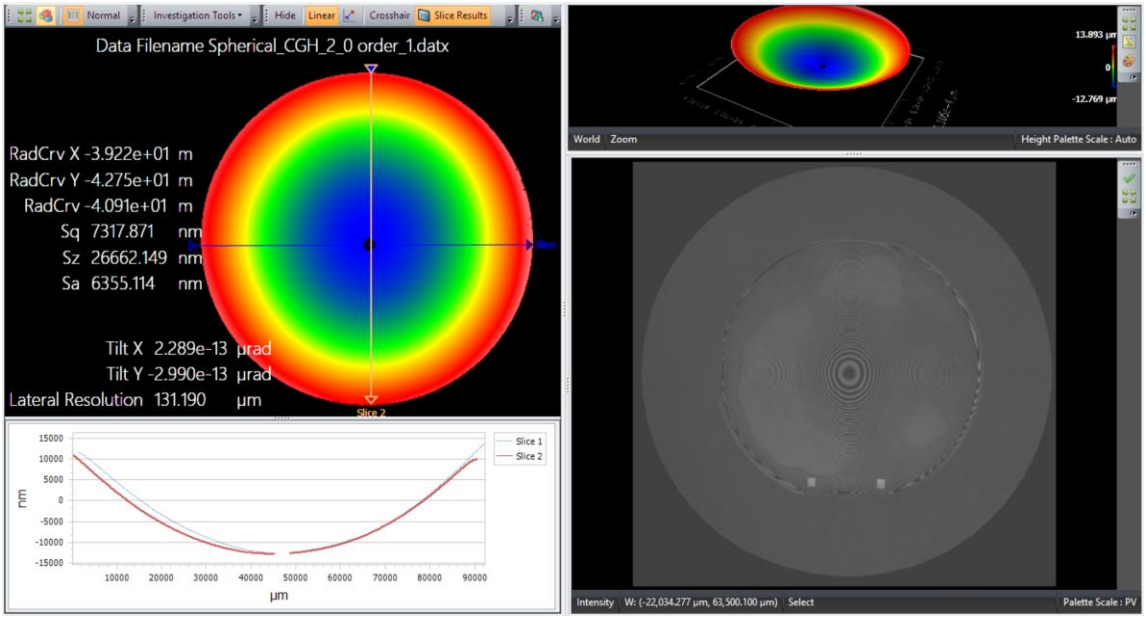

Figure 9: The shape of the SCGH sample #2 as measured in the zero-order arrangement with the Fizeau interferometer equipped with a plane transmission reference. The best fit plane surface is detrended.

Note that in the current SCGH design, there is no easy way to block any unwanted orders. Due to the simple on-axis design of this SCGH, light from all diffraction orders returns to the interferometer when we illuminate the CGH. An improved design of the SCGH, which permits the spatial filtering unwanted orders would require a tilt term in the phase. We will describe in the discussion of the first-order measurements, how the current simplified design also leads to undetermined

height data over the SCGH central area due to very low fringe contrast. In addition, we are presently developing improved SCGH/BPRA samples using significantly thicker substrates with better surface quality.

4.3 First-order measurements with the spherical CGH samples before fabrication of the HR-BPRA pattern using spherical-wavefront Fizeau interferometry

Figure 10 illustrates the above-mentioned contrast effect of undetermined data over the SCGH #1 central area when measuring in the first order using various settings of the Fizeau interferometer. With the standard settings used for the zero-order measurements (Figure 9), the undetermined area is very large (Figure 10a). Therefore, we performed a thorough optimization of the measurement settings to minimize the size of the central undetermined area (Figure 10b).

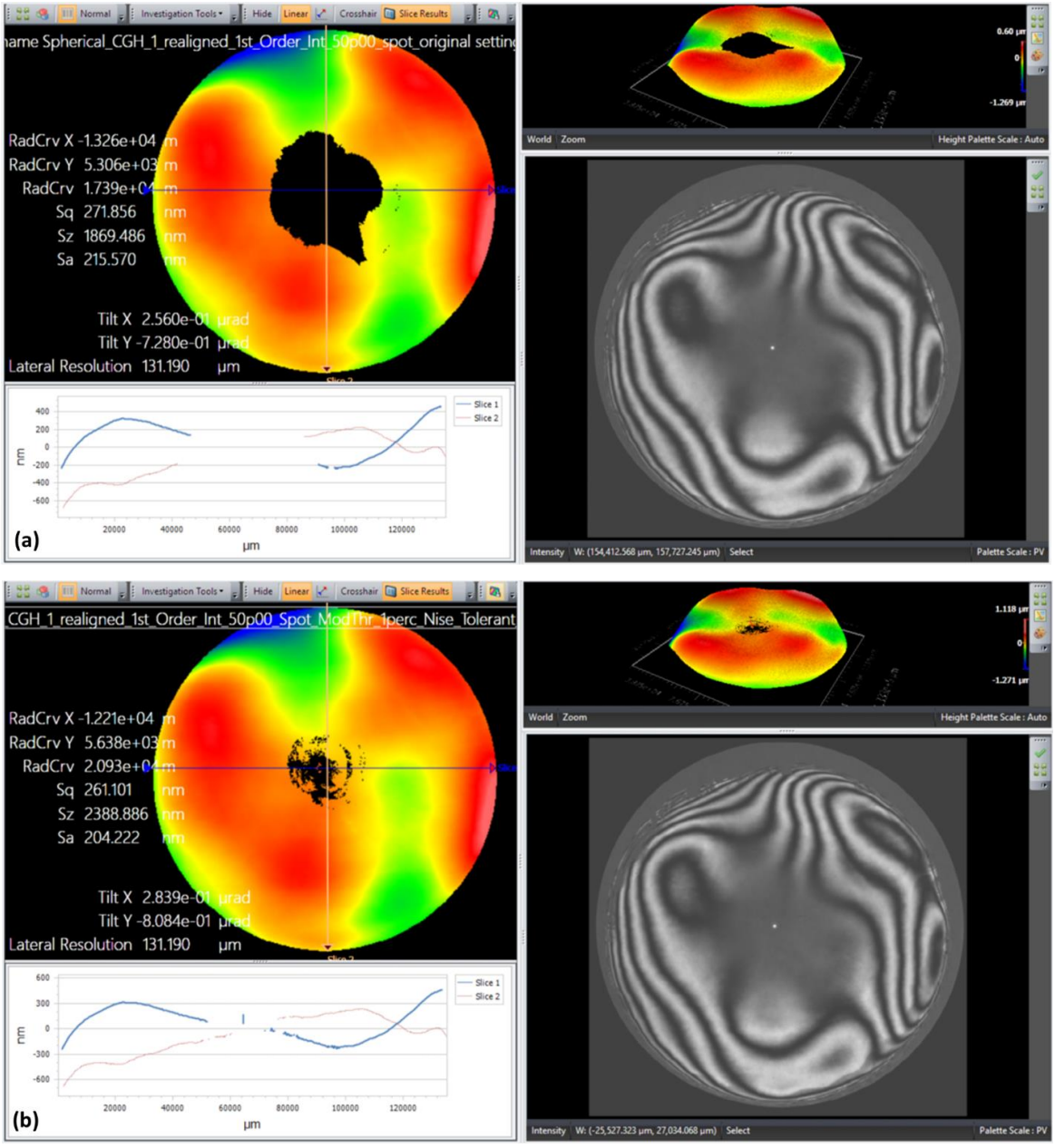

Figure 10: Screenshots of the interferometer software reproducing the results of the first-order measurements with the SCGH sample #1 before BPRA patterning performed with the Fizeau interferometer using the (a) original and (b) optimal setting. The best fit plane surface is detrended.

Figure 11 shows the shape of the SCGH sample #2 as measured in the first-order arrangement with the Fizeau interferometer using the optimal measurement setting. One can see that the unrecovered area at the SCGH #2 center is noticeably smaller than that of the sample #1 (compare with Figure 10). For this reason we will concentrate on the analysis and discussion of the Fizeau interferometry data obtained with the SCGH sample #2 before and after fabrication of the HR-BPRA pattern.

There is an interesting question about the possibility of improving the PSD measurement of the SCGH/BPRA first order by subtracting (after the appropriate lateral recalibration) the zero-order SCGH (without BPRA) surface shape. A positive (however only a qualitative) answer to this question can be obtained from a comparison of the SCGH #2 shapes measured in the Fizeau interferometry in the first order (Figure 9) and the zero order (Figure 11), which is shown in Figure 12.

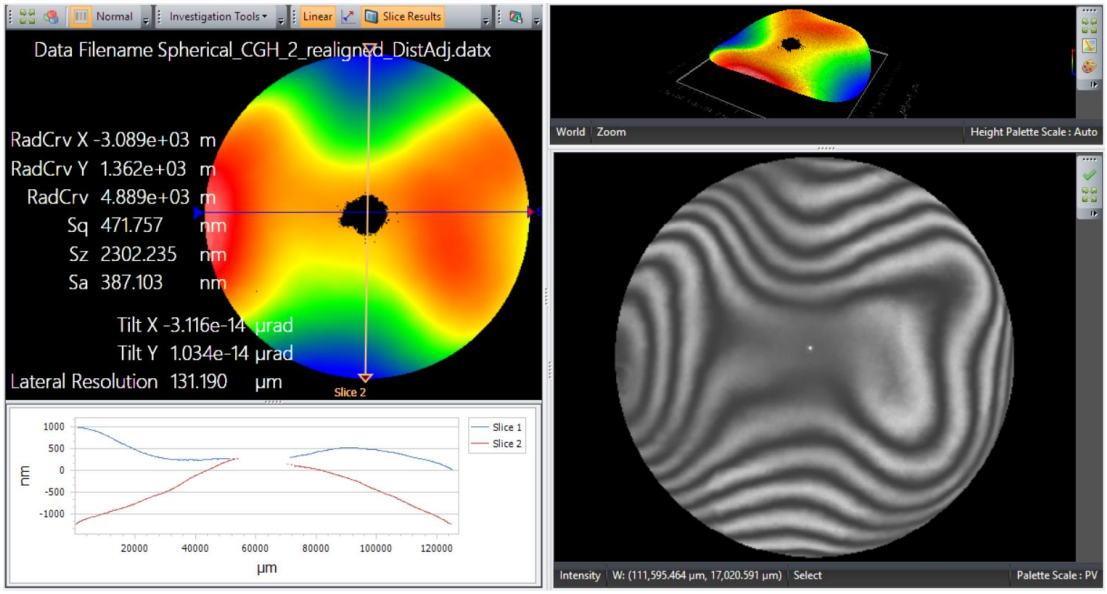

Figure 11: The shape of the SCGH sample #2 as measured in the first diffraction order with the Fizeau interferometer equipped with a spherical transmission reference. The optimal measurement settings were used for this measurement. The best fit plane is subtracted. Note that the unrecovered area at the SCGH center is noticeably smaller than that of the sample #1 (compare with Figure 10b).

In Figure 12, the shapes of the SCGH sample #2 as measured in zeroth and first diffraction order with the Fizeau interferometer are shown. In both cases, the best fit eighth-order polynomial surfaces are subtracted. In order to account for the reversal of the first-order surface shape of concave spherical optics placed downstream of the focus position of a spherical transmission reference, the interferometer software screenshot of the first order (Figure 12b) is rotated by 180 degrees. One can see the similarity between the residual surface topology obtained in the zero and first order measurements.

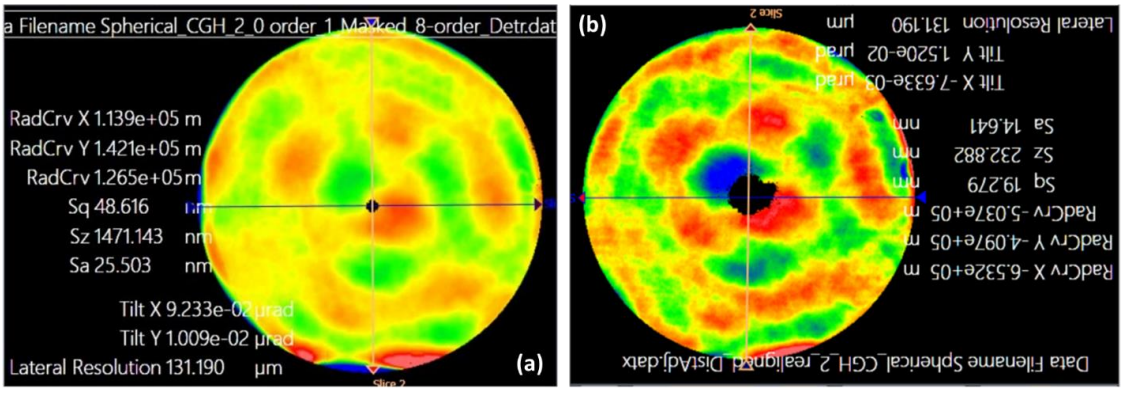

Figure 12: The SCGH sample #2 measured in the (a) first and (b) zeroth diffraction order with the Fizeau interferometer equipped with a spherical and plane transmission reference. The best fit eight-order polynomial surfaces are subtracted.

4.4 First-order measurements with the spherical CGH samples after fabrication of the HR-BPRA pattern using spherical-wavefront Fizeau interferometry

After the HR-BPRA pattern was processed on the top of the SCGH samples as described in Sec. 2, we repeated the first-order measurements with SCGH/BPRA samples using spherical-wavefront Fizeau interferometry in the arrangement shown in Figure 8. A screenshot of the interferometer software displaying the measurement with the SCGH/BPRA sample #2 is shown in Figure 13. Again, the best fit eighth-order polynomial surface is subtracted. In addition to height maps and cross-sections, the screenshot in Figure 13 displays slice and y-average 1D power spectral densities (PSD). As the interferometer software's PSD algorithm is proprietary and undocumented, we do not know how this code accounts for the missing height values at the center. We are presently adapting our own 1D and 2D PSD routines to handle areas of missing data in a useful manner.

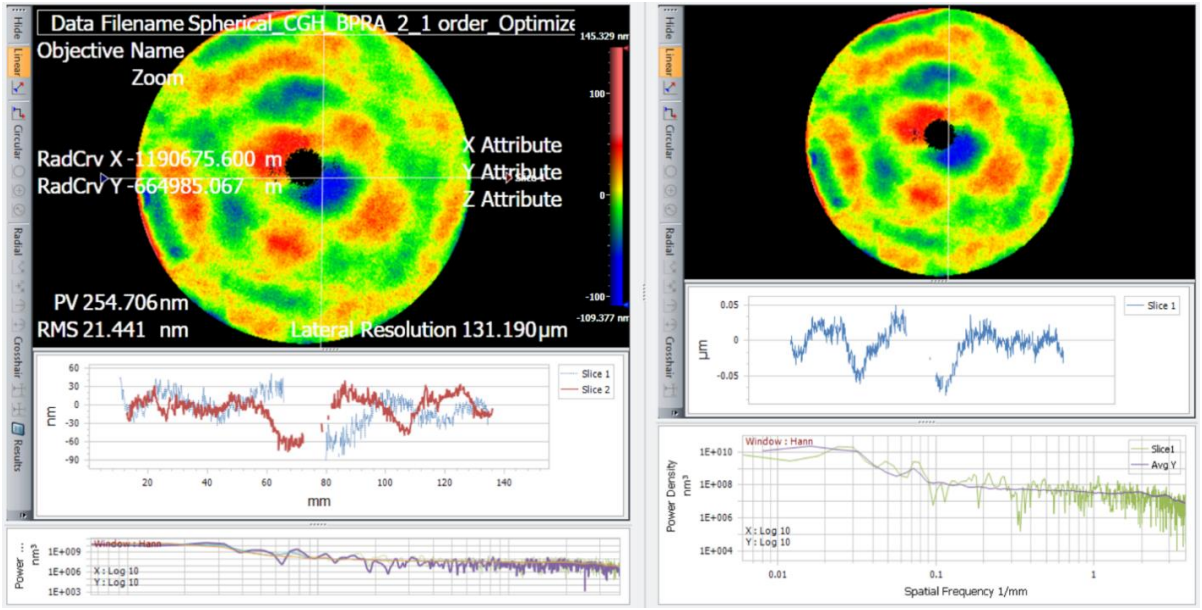

Figure 13: Screenshots of the interferometer software reproducing the results of the first-order measurements with the SCGH/BPRA sample #2 performed with the Fizeau interferometer using the optimal measurement settings. The best fit eighth-order polynomial surface is subtracted.

In order to understand the contribution to the PSD in Figure 13 of the BPRA height topography, we compare it with the PSD measured with the same SCGH sample before fabrication of the BPRA pattern in Figure 14. The PSD of the sample without the BPRA pattern is more than an order of magnitude smaller at higher spatial frequencies, indicating that the BPRA pattern is the dominant source of height variation at these frequencies.

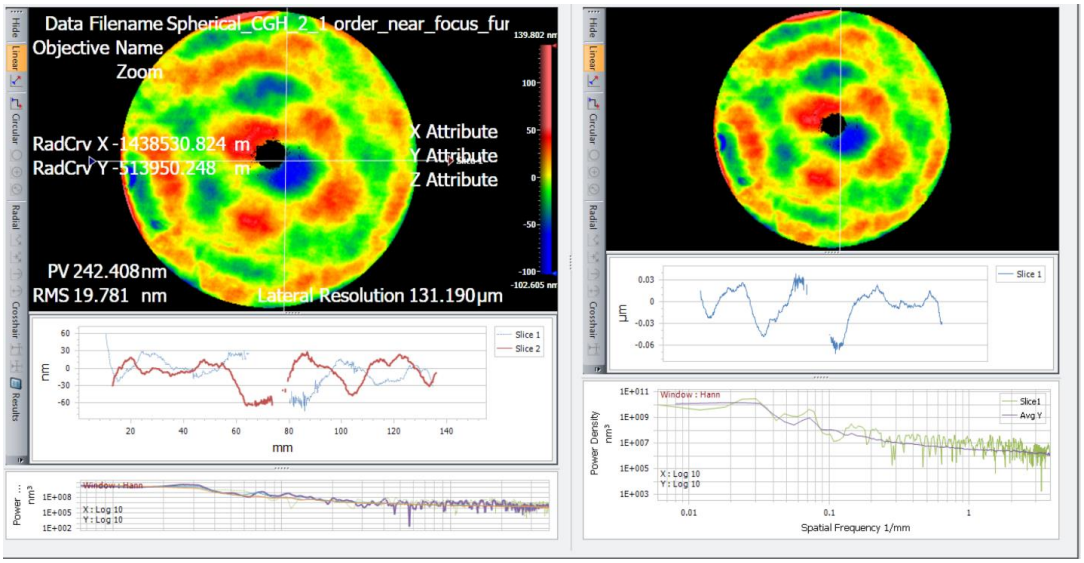

Figure 14: Screenshots of the interferometer software reproducing the results of the first-order measurements with the SCGH sample #2 before fabrication of the BPRA pattern. The best fit eighth-order polynomial surface is subtracted.

At about 0.07 1/mm there is a peak in the PSD for measurements both with and without the BPRA pattern due to large-scale surface-height variation visible in both measurements. This peak can be removed, isolating the contribution from the BPRA, by using the measurement without the BPRA as a reference, subtracting the height profile from the measurement with the BPRA before taking the PSD.

Figure 15 shows the difference of the height distributions in Figure 13 and Figure 14, as well as the corresponding averaged PSD_Y. As expected, the PSD distribution of the difference has noticeably smoother behavior in the middle spatial frequency range.

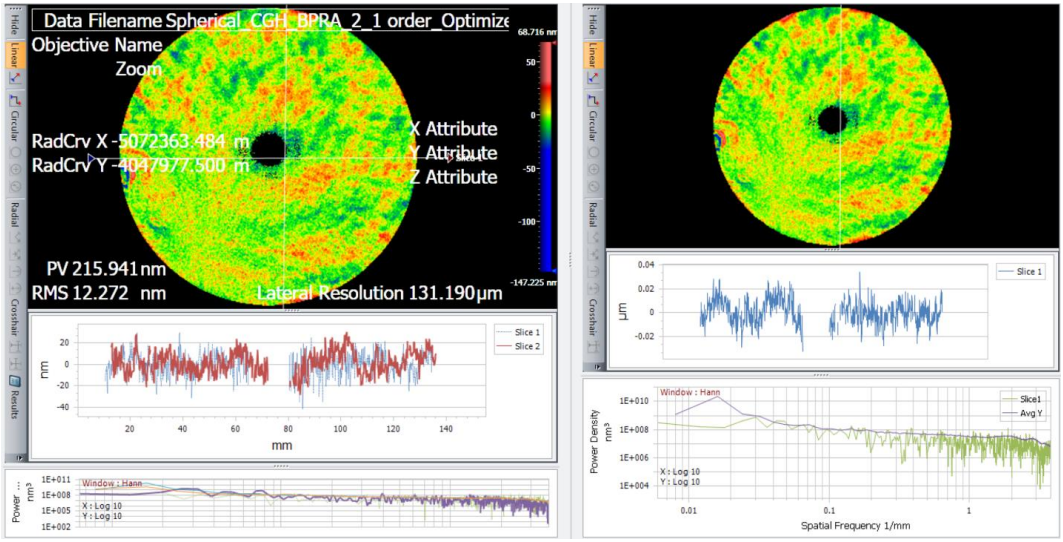

Figure 15: Screenshots of the interferometer software reproducing the difference of the surface height distributions in Figure 13 and Figure 14 obtained with the BPRA-patterned and BPRA-free SCGH sample #2. The PSD of the difference is noticeably smoother middle spatial frequency behavior than that of the original data.

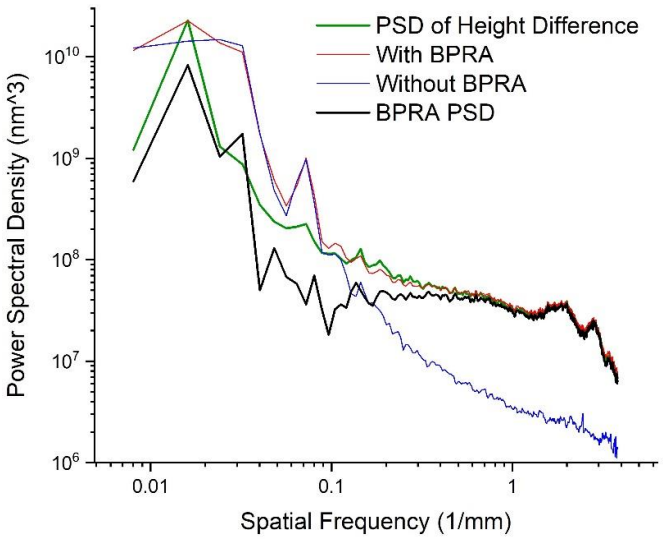

Figure 16: The averaged PSDY of the SCGH sample #2 after (the red line) and before (the blue line) fabrication of the HR-BPRA pattern, as well as the PSDY of the BPRA topography itself (the bold black line) evaluated as a difference of the first two PSDs, and the averaged PSDY distribution of the height difference of the corresponding measurements.

The results of the described proof-of-principle test with the HR-BPRA ITF calibration artifact on the SCGH is summarized in Figure 16. Figure 16 reproduces the averaged PSD_Y distributions of the sample #2 before and after HR-BPRA patterning, as well as their difference in the spatial frequency domain. This is the most reliable measure of the BPRA PSD, and thus represents the ITF of the Fizeau interferometer in the arrangement used to make the measurements. For reference, we also show the averaged PSD_Y distribution of the height difference of the measurements.

Note that the resulting BPRA PSD, shown in Figure 16 with the bold black line, is very similar to that measured for ITF calibration of a Fizeau interferometer equipped with a plane transmission reference for measurements of plane optics (see, for example, Refs. [2,3]). In that case, as well as in the case of cylindrical wavefront interferometry discussed in Ref. [4], the high spatial frequency irregularity of the PSD distribution has been shown to be an indication of inappropriate adjustment of the focus of the interferometer. Most probably, this is also the case in the measurements depicted in Figure 13. Further investigation in this direction is in progress.

5. CONCLUSIONS

Summarizing the results of the proof-of-principle tests of the SCGH/BPRA sample in application to the spherical wavefront Fizeau interferometry discussed throughout this section, we conclude that the suggested approach of the fabrication of the ITF calibration artifacts as a combination of the CGH and BPRA patterns developed on a plane substrate is a powerful new way to measure the instrument transfer function of an interferometer with a transmission sphere and, potentially, with any other nulling optics, including a cylindrical wavefront interferometer, such as the one at the NASA Metrology Lab [4].

The demonstrated approach also solves another problem with transmission spheres, namely that of keeping all areas of a curved test part within the focus of the transmission sphere, especially for faster transmission spheres. Patterning the BPRA on a zone plate not only obviates the need to fabricate a BPRA on a curved part to test a curved wavefront, the BPRA will be in focus everywhere.

ACKNOWLEDGEMENTS

This work was partially supported by the U. S. Department of Energy under contract number DE-AC02-05CH11231 and by the NASA SBIR program under award number 80NSSC22PB039. Research at the Advanced Light Source and the Molecular Foundry at Lawrence Berkeley National Laboratory are supported by the Office of Science, Office of Basic

Energy Sciences, and Material Science Division of the U.S. Department of Energy under Contract No. DE-AC02-05CH11231.

DISCLAIMER

REFERENCES

[1]V. V. Yashchuk, K. Munechika, S. Rochester, W. Chao, I. Lacey, C. Pina-Hernandez, and P. Z. Takacs, "Reliability investigation of the instrumentation transfer function calibration technique based on binary pseudo-random array standards," SPIE Proc. 12240, 122400D/1-11 (2022); doi: 10.1117/12.2633476.

[2] V. V. Yashchuk, S. Babin, S. Cabrini, W. Chao, U. Griesmann, I. Lacey, S. Marchesini, K. Munechika, C. Pina-Hernandez, and A. Roginsky, "Binary pseudorandom array test standard optimized for characterization of large field-of-view optical interferometers," Proc. SPIE 11490, 114900W/1-8 (2020); doi: 10.1117/12.2568309.

[3] V. V. Yashchuk, S. Babin, S. Cabrini, U. Griesmann, I. Lacey, K. Munechika, C. Pina Hernandez, and Q. Wang, "Characterization and operation optimization of large field-of-view optical interferometers using binary pseudorandom array test standard," Proc. SPIE 10749, 107490R/1-13 (2018); doi: 10.1117/12.2322011.

[4] K. Munechika, S. Rochester, M. P. Biskach, W. Chao, U. Griesmann, I. Lacey, C. Pina-Hernandez, A. Numata, P. Z. Takacs, K. Yamada, W. W. Zhang, and V. V. Yashchuk, "Binary pseudo-random array (BPRA) for inspection and calibration for cylindrical wavefront interferometry," SPIE Proc. 12677, 1267708/1-15 (2023); doi: 10.1117/12.2677966.

[5] Burge, James H. "Applications of computer-generated holograms for interferometric measurement of large aspheric optics." *International Conference on Optical Fabrication and Testing*. Vol. 2576. SPIE, 1995.